OH column abundance over Table Mountain Facility, California: Intra-annual variations and comparisons to model predictions for 1997–2001

Franklin P. Mills,[1,2] Richard P. Cageao,[1] Stanley P. Sander,[1,3,4] Mark Allen,[1,4] Yuk L. Yung,[4] Ellis E. Remsberg,[5] James M. Russell III,[6] and Ulf Richter[3]

Received 4 February 2003; revised 14 July 2003; accepted 11 August 2003; published 24 December 2003.

[1] Measurements of the OH column abundance over the Jet Propulsion Laboratory's Table Mountain Facility (TMF) have been made since July 1997 at 10°–80° solar zenith angle using a Fourier transform ultraviolet spectrometer. The measured OH column at any solar zenith angle is typically larger in the afternoon than in the morning. The variations observed in the OH column abundance appear to result from changes in atmospheric conditions on a daily or longer timescale. The larger observed variations are statistically significant. Sensitivity coefficients describing how the OH column abundance is expected to change in response to changes in the concentrations of H_2O, O_3, NO, CO, and CH_4 have been calculated on the basis of an analytic model. On the basis of these sensitivity coefficients and Halogen Occultation Experiment observations of O_3, the net sensitivity of the OH column abundance to variations in O_3 should be close to zero. The observed OH column abundance over TMF increased by about 25% from July 1997 to December 2001. This interannual trend in OH column abundance is not consistent with calculations that incorporate observed trends in H_2O and O_3 and is at least a factor of 2 larger than the calculated difference between solar minimum and maximum. Comparisons between measured and calculated normalized OH column abundances suggest that the sensitivity of OH to variations in H_2O may be a factor of 2 larger than predicted in present models and that there is some other major driver for the observed variability in the OH column abundance that was not included in the present analysis. *INDEX TERMS:* 0317 Atmospheric Composition and Structure: Chemical kinetic and photochemical properties; 0340 Atmospheric Composition and Structure: Middle atmosphere—composition and chemistry; 0394 Atmospheric Composition and Structure: Instruments and techniques; 7536 Solar Physics, Astrophysics, and Astronomy: Solar activity cycle (2162); *KEYWORDS:* hydroxyl, mesosphere, photochemistry

Citation: Mills, F. P., R. P. Cageao, S. P. Sander, M. Allen, Y. L. Yung, E. E. Remsberg, J. M. Russell III, and U. Richter, OH column abundance over Table Mountain Facility, California: Intra-annual variations and comparisons to model predictions for 1997–2001, *J. Geophys. Res.*, *108*(D24), 4785, doi:10.1029/2003JD003481, 2003.

1. Introduction

[2] Although it contains only about 15% of the total ozone column, the distribution of ozone in the 30–70 km altitude region of the atmosphere affects global stratospheric temperatures and circulation [*Müller et al.*, 1999]. This region also is believed to be the region in which the first evidence for a recovery of ozone toward pre-industrial levels may be observed [*Hofmann et al.*, 1999]. To properly identify the recovery of ozone from anthropogenic influences, the natural chemistry must be understood. Ozone loss in the upper stratosphere and lower mesosphere is believed to be dominated by reactions involving chlorine oxides (ClO_x) and odd-hydrogen species (HO_x = H + OH + HO_2 + H_2O_2), so a good understanding of both HO_x and ClO_x chemistry is needed. Measurements of OH are a direct probe of the chemistry in this region because OH is a key species in many of the most important reactions. The most recent observations of OH, HO_2, and O_3 have not agreed satisfactorily with photochemical model calculations based on existing laboratory data [*Jucks et al.*, 1998; *Sandor and Clancy*, 1998; *Conway et al.*, 2000], and significant revisions to the standard chemistry for the mesosphere and upper stratosphere have been proposed. Those studies, however, examined measurements collected over limited

[1]Jet Propulsion Laboratory, California Institute of Technology, Pasadena, California, USA.
[2]Now at Research School of Physical Sciences and Engineering, Australian National University, Canberra, ACT, Australia.
[3]Division of Engineering and Applied Science, California Institute of Technology, Pasadena, California, USA.
[4]Division of Geological and Planetary Sciences, California Institute of Technology, Pasadena, California, USA.
[5]NASA Langley Research Center, Hampton, Virginia, USA.
[6]Center for Atmospheric Sciences, Hampton University, Hampton, Virginia, USA.

0148-0227/03/2003JD003481

periods of time, so they have sampled only a small fraction of the range of conditions that may exist in the stratosphere and mesosphere.

[3] One additional tool that may be used for analyzing the daytime photochemistry in the upper stratosphere and mesosphere is column-integrated measurements of OH abundance collected throughout the day for at least several days per month over an extended period of time. A large majority of the OH column is at 30–70 km altitude, so the OH column abundance should be sensitive to the photochemical state of this region. This paper describes the first 3.5 years of measurements of the OH column abundance over the Jet Propulsion Laboratory's (JPL) Table Mountain Facility (TMF) at 34.4N, −117.7E. An analytical photochemical model [*Pickett and Peterson*, 1996] was updated and used to determine the primary geophysical parameters that should control variations in OH column abundance. These were found to be O_3 and H_2O. We then compare the observed intra-annual variations in OH column to calculations based on observed variations in the precursor species, O_3 and H_2O, with the aid of the updated analytical photochemical model.

[4] Profiles for OH in the stratosphere and mesosphere have been measured by several groups since the early 1980s [*Canty et al.*, 2000]. Three recent studies [*Jucks et al.*, 1998; *Conway et al.*, 2000; *Summers et al.*, 1997] have been particularly important because OH profiles were measured simultaneously with those of other relevant species (O_3, H_2O, and/or HO_2). These three studies concluded that present photochemical models do not accurately capture the actual HO_x chemistry in the stratosphere and mesosphere. The most recent study [*Conway et al.*, 2000] concluded that none of the previously proposed revisions to the accepted chemical kinetic rates could satisfactorily explain the differences between calculated and measured OH abundances throughout the upper stratosphere and mesosphere.

[5] OH column measurements have been made over Fritz Peak Observatory, Colorado, (FPO) since 1977 [*Burnett and Burnett*, 1996], over Tokyo, Japan, in 1992–1995 [*Iwagami et al.*, 1998], and over Socorro, New Mexico (NMT), since 1996 [*Burnett and Minschwaner*, 1998; *Canty et al.*, 2000]. Long-term measurement records, such as these, are necessary for determining statistically significant correlations between OH column abundance and climatic or dynamic changes in the upper stratosphere and mesosphere. Temporal variations in the OH column abundance on seasonal to decadal timescales have been reported for all three sites [*Burnett and Burnett*, 1996; *Iwagami et al.*, 1998]. These temporal variations have not been satisfactorily explained in terms of relevant geophysical parameters, partly because of the difficulties involved in interpreting column measurements.

[6] The column abundance of OH over Table Mountain Facility (TMF), California, has been measured regularly since July 1997 using the Fourier transform ultraviolet spectrometer [*Cageao et al.*, 2001]. One motivation for initiating these measurements is the large (and unexplained) differences among the previous OH column measurements and the significant differences between all of the OH column measurements and model calculations [*Iwagami et al.*, 1998]. For example, the annual average OH column observed for 1998–2000 over TMF is 10–20% larger than that observed by another group over Tokyo for 1992–1995; 30–65% smaller than that observed by other groups over Colorado and New Mexico for 1980–1996; and 15–30% smaller than calculated by photochemical models [*Mills et al.*, 2002]. However, three different types of instruments and two different measurement approaches were used at these four sites. All OH column measurements require a method for inferring (or removing) the exoatmospheric solar spectrum which has deep Fraunhofer lines that interfere with the terrestrial OH features. As discussed by *Cageao et al.* [2001] and *Mills et al.* [2002], the measurement and analysis methods used for the TMF spectral data are extremely effective in canceling the strong solar Fraunhofer lines which interfere with terrestrial OH absorption measurements. All of the OH column measurements are subject to systematic uncertainties. Some, such as the uncertainties on the oscillator strengths for the OH lines used for the column observations, are the same for all of the measurement sites. Others, such as corrections for stray light, will differ for each site. To minimize the influence of possible systematic errors, the analysis in this paper will focus on normalized deviations of the OH column from the average observed over TMF. Time-dependent modeling of the diurnal variation and the absolute OH column abundance are underway and will be published when completed.

[7] The goals for this paper are to characterize the first 3.5 years of the TMF OH column measurements and assess how well model calculations can reproduce the observed, statistically significant variations in the OH column. Observed intra-annual variations in O_3 and H_2O in the stratosphere and mesosphere derived from measurements by the Halogen Occultation Experiment (HALOE) [*Russell et al.*, 1993] on the Upper Atmosphere Research Satellite (UARS) will be used to calculate expected intra-annual variations in the OH column abundance. These calculations are then compared to the observed intra-annual variations in the OH column.

[8] Section 2 briefly describes the OH column measurements made over TMF. Section 3 presents our analysis of intra-annual variations in the OH column over TMF. Section 4 describes the analytic photochemical model, and section 5 how it was used to derive sensitivity coefficients for the primary geophysical parameters governing the OH column abundance in models: H_2O and O_3 concentrations. The sensitivity coefficients quantitatively derived from the analytic model relate variations in H_2O and O_3 concentrations to the predicted effect on the OH column abundance. Section 6 uses these sensitivity coefficients to compare the observed variations in the OH column over TMF with predictions based on observed variations in H_2O and O_3 concentrations near TMF.

2. Observations

[9] Since July 1997, the OH column abundance has been measured over TMF using the Fourier transform ultraviolet spectrometer (FTUVS) [*Cageao et al.*, 2001; *Mills et al.*, 2002]. Figure A1 in the auxiliary material[1] shows the dates

[1] Auxiliary material is available via Web browser or via Anonymous FTP from ftp://agu.org/apend/jd/2003JD003481/. Information on searching and submitting electronic supplements is found at http://www.agu.org/pubs/esupp_about.html.

and solar zenith angles (SZA) for morning measurements. Afternoon data coverage is similar, Figure A2. The collecting optics for the FTUVS were upgraded in September–December 1999 so no data were collected during this period.

[10] The FTUVS acquires spectra of the Sun from the ground by viewing the east and west limbs of the Sun, alternately, for 15 min each. The Doppler shift induced by the rotation of the Sun shifts the solar Fraunhofer lines observed at the east and west limbs of the Sun relative to the telluric OH lines. A properly shifted ratio of a pair of east and west limb spectra then removes the solar Fraunhofer lines and leaves only features due to the telluric OH. The OH features are fit with a calculated spectrum to derive the line-of-sight OH column abundance. The calculated spectrum includes a model of the instrument line shape and the expected Doppler broadening based on a standard atmospheric temperature profile. The line-of-sight OH column abundance is divided by cos(SZA) to determine the vertical OH column abundance [*Cageao et al.*, 2001]. The FTUVS at TMF has an unapodized spectral resolving power near 500,000 and integration time of 30 min for a pair of east and west solar limb spectra [*Cageao et al.*, 2001]. The measured absorption is converted to OH column abundance using the oscillator strengths for the individual rotational lines in the $A^2\Sigma^+ \leftarrow X^2\Pi(0, 0)$ band for OH [*Cageao et al.*, 1997]. The band oscillator strength used in the present analysis is within 0.5% of those used by other groups [*Burnett and Burnett*, 1981; *Iwagami et al.*, 1995]. The OH lines observed by the FTUVS are optically thin (total column absorption ~1%) so the measurements are sensitive to the entire OH column.

[11] At least seven OH lines in the $A^2\Sigma^+ \leftarrow X^2\Pi(0, 0)$ band are observed. This paper focuses on results from the $P_1(1)$ line (32440.5741 cm^{-1}) and the $Q_1(2)$ line (32458.5918 cm^{-1}) [*Stark et al.*, 1994]. The $P_1(1)$ line was used by other groups because the solar spectrum has less curvature near the $P_1(1)$ line and it gave the most reliable ("stable") results [*Iwagami et al.*, 1995; *Notholt et al.*, 1997]. Observations of the $Q_1(2)$ line have not been reported by previous investigators. The TMF annual averages derived from the $P_1(1)$ and $Q_1(2)$ lines agree [*Mills et al.*, 2002]. The other five OH lines observed at TMF are weaker and have greater interference from solar lines. Reliable retrieval techniques using the weaker lines are still being developed and were not included in the present analysis.

[12] Figures A3 and A4 summarize all of the measurements of OH column abundance that were made over TMF from July 1997 to December 2001. A strong, approximately linear dependence on SZA is present in the TMF data, as has been reported for other data sets [*Burnett and Burnett*, 1981]. The range of observable SZAs for each season is indicated by the symbols, and Figure A3 indicates the variability within each season is comparable in magnitude to that between seasons at any given SZA.

[13] The primary source of uncertainty in the measured OH column is the spectral fit [*Cageao et al.*, 2001]. Figure A5 is a histogram of the $2\sigma_{sf}$ spectral fit uncertainty for $P_1(1)$ data collected after June 1997. Figure A6 shows the spectral fit uncertainties for $Q_1(2)$ data. The median spectral fit uncertainty ($2\sigma_{sf}$) for $P_1(1)$ data is 14% and for $Q_1(2)$ data is 17%. The $2\sigma_{ro}$ random uncertainty from all other sources (root-sum-square) is 14% [*Cageao et al.*, 2001], and the median of the total (root-sum-square) random uncertainty ($2\sigma_r$) is 20%. The $2\sigma_s$ systematic uncertainty from all sources (root-sum-square) is estimated to be 12% [*Cageao et al.*, 2001].

3. Measurement Results

[14] The OH column abundance observed over TMF (Figures A3 and A4) is a strong function of solar zenith angle (SZA) but statistically significant variations are observed at all SZA. To characterize the observed variations and minimize the susceptibility to systematic uncertainties [*Mills et al.*, 2002], the typical solar zenith angle dependence must be removed. This has been accomplished by calculating linear least squares fits, separately, for the morning and afternoon measurements (Figures 1 and A7). The measured OH column abundances are then divided by the appropriate empirical fit. Hereinafter, the resultant fractional deviations from the empirical fits are referred to as "normalized OH column abundances."

[15] Figures 1 and A7 have two different empirical fits. The linear fit was calculated for 10°–65° solar zenith angle where the spectra have the best signal-to-noise ratio so the measured OH columns have the best quality. The second-order polynomial fit was calculated for 10°–85° solar zenith angle. The two fits agree to within the uncertainty on the linear fit for most of the 10°–65° solar zenith angle range, so a higher-order fit is not justified and we believe the linear fit adequately describes the overall TMF data set for 10°–65° solar zenith angle even though model calculations [*Canty et al.*, 2000] predict a non-linear relationship between OH column and solar zenith angle. The best linear fits for the $P_1(1)$ OH column measurements over TMF for July 1997 to December 2001 at 10°–65° SZA with spectral fit uncertainty ≤36% are given by equations (1) and (2).

$$m_1 = -5.87(\pm 0.29)10^{11} \times \mathrm{SZA} + 7.60(\pm 0.14)10^{13} \quad (1)$$

$$a_1 = -4.63(\pm 0.32)10^{11} \times \mathrm{SZA} + 7.38(\pm 0.16)10^{13} \quad (2)$$

where SZA = solar zenith angle, m_1= morning $P_1(1)$ OH column (cm^{-2}), and a_1 = afternoon $P_1(1)$ OH column (cm^{-2}). The best linear least squares fits for the $Q_1(2)$ OH column measurements over TMF for July 1997 to December 2001 at 10°–65° SZA with spectral fit uncertainty ≤41% (Figures A8 and A9) are given by equations (3) and (4).

$$m_0 = -6.32(\pm 0.35)10^{11} \times \mathrm{SZA} + 8.15(\pm 0.17)10^{13} \quad (3)$$

$$a_0 = -5.60(\pm 0.39)10^{11} \times \mathrm{SZA} + 8.31(\pm 0.19)10^{13} \quad (4)$$

where m_0 = morning $Q_1(2)$ OH column (cm^{-2}), and a_0 = afternoon $Q_1(2)$ OH column (cm^{-2}). The annual average OH column derived from observations of the $P_1(1)$ and $Q_1(2)$ OH lines (as described by m_1, a_1, m_0, and a_0) agree to within their mutual uncertainties [*Mills et al.*, 2002], and the recently revised line strengths for the two OH lines [*Gillis et al.*, 2001] are expected to improve the agreement of these

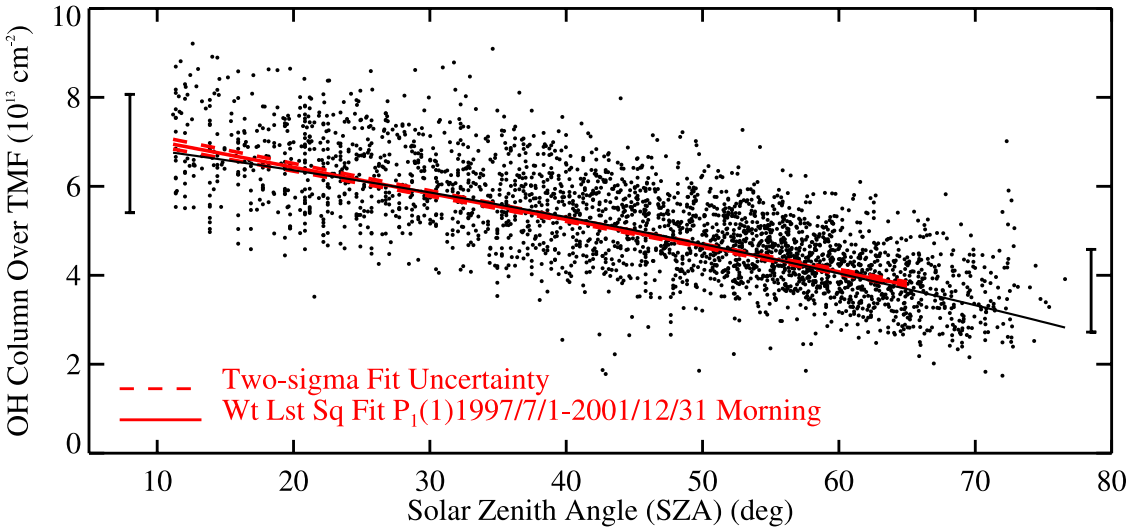

Figure 1. Morning OH column measurements with spectral fit uncertainty smaller than 36% as a function of SZA over TMF for July 1997 to December 2001 for the $P_1(1)$ OH line. Each point on the plot is one measurement of the OH column abundance as derived from a pair of 15-min integrations on each limb of the Sun. The vertical bars at each end illustrate the typical $2\sigma_r$ random uncertainty for an OH column measurement at 10°–20° and 65°–75° SZA, respectively. Points and vertical bars are the same as in Figure A3, but excluding points with large spectral fit uncertainties. The solid black curve is the best second-order fit to the data. The solid red line is the best linear fit to the data. The short-dashed red lines are the 2σ uncertainties on the best linear fit. All fits and the uncertainties on the fits were calculated via a weighted least squares singular value decomposition technique [*Press et al.*, 1989, chapter 14]. The second-order and linear fits are almost indistinguishable for most SZA. The smallest OH column abundances at 25°–65° SZA in this figure were measured after a solar storm in April 2000, but the spectral fit uncertainties for the OH column abundances measured after the April 2000 solar storm (Figure A3) are generally larger than the 36% limit used to select data for inclusion in this figure.

annual averages by about 2–3%. The shallower slope for the fit to the afternoon OH column (when compared to the morning OH column) is true for almost all months for both the $P_1(1)$ and $Q_1(2)$ lines.

[16] Deviations from the empirical fits shown in Figures 1 and A7 are believed to be primarily due to geophysical variations in the atmosphere. To facilitate detection of variability patterns on timescales longer than 1 day and to enable comparison with model calculations, the normalized $P_1(1)$ OH column abundances were averaged to create morning and afternoon daily averages (Figure A10). Statistically significant deviations from the empirical mean of up to +40% and −50% are observed and variability on at least week-to-week or monthly timescales is readily apparent.

[17] Inspection of the normalized $P_1(1)$ OH column abundances showed no obvious dependence on solar zenith angle, and correlation tests among the normalized $P_1(1)$ OH abundances for most solar zenith angles showed high correlations. The morning and afternoon daily average normalized $P_1(1)$ OH columns also are highly correlated (Figure 2), with a slope near unity and an intercept near zero (equation (5)).

$$a_{1n} = 0.95(\pm 0.06)m_{1n} + 0.01(\pm 0.01) \quad (5)$$

where a_{1n} = daily average normalized afternoon $P_1(1)$ OH column abundance and m_{1n} = daily average normalized morning $P_1(1)$ OH column abundance. The only $P_1(1)$ data with a lower degree of correlation than is shown in Figure 2 are data collected at $\gtrsim 50°$ solar zenith angle in the morning. Morning data collected at solar zenith angles $\geq 45°$ over FPO have been the subject of several studies [*Burnett and Minschwaner*, 1998]. For the TMF data set, however, these early morning data have the lowest signal-to-noise ratios because they have the longest slant paths through the atmosphere and the OH column abundance is smallest. (Broadband atmospheric attenuation, such as Rayleigh scattering, and O_3 absorption near 308 nm is largest at the longest slant paths.) Thus the early morning data have the poorest quality spectral fits. On the basis of the lack of a clear temporal pattern in Figure A11, we believe that the lower degree of correlation between early morning TMF data and TMF data collected throughout the remainder of the day is due to the poorer quality of the early morning measurements.

[18] The high degree of correlation observed among OH column variations at all solar zenith angles and between morning and afternoon strongly suggest that the observed variations are not random fluctuations. These results also indicate the daily average normalized $P_1(1)$ OH column abundances adequately capture the variability in the measured $P_1(1)$ OH column abundances and suggest that the observed changes in the normalized $P_1(1)$ OH column occur "uniformly" throughout the day. On the basis of the high correlation between the morning and afternoon averages for the $P_1(1)$ OH line measurements, the normalized OH columns from the entire day have been averaged (Figure 3). A statistically significant increase in the OH

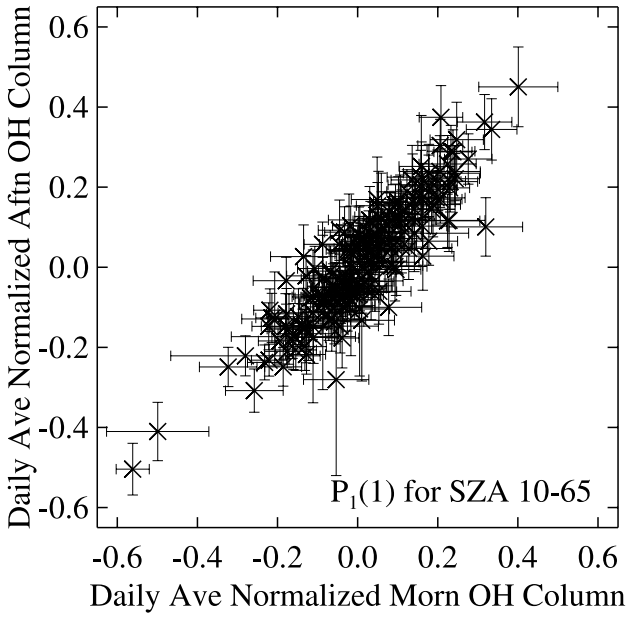

Figure 2. Scatterplot of the morning and afternoon 1-day averages (Figure A10), showing the high degree of correlation between the 1-day average normalized OH column abundance measured in the morning and afternoon. The horizontal axis is the average for each day of the normalized morning OH column abundance for the $P_1(1)$ OH line data collected at 10°–65° SZA between July 1997 and December 2001. The vertical axis is the average for each day of the normalized afternoon OH column abundance for the same conditions. Uncertainties are $2\sigma_r$ uncertainties on the mean for each day [*Bevington*, 1969, chapter 5]. The weighted linear least squares fit through the measurements [*Press et al.*, 1989, chapter 14] is described by $a_{1n} = (0.95 \pm 0.06) * m_{1n} + (0.01 \pm 0.01)$, where a_{1n} is the normalized afternoon OH column and m_{1n} is the normalized morning OH column.

column abundance over TMF from 1997 to 2001 is evident and the linear fit shown in Figure 3 indicates the OH column abundance over TMF increased by about 25% (difference divided by mean) from July 1997 to December 2001. The smallest OH column abundances were recorded during one week periods in April and July 2000, shortly after intense solar storms. The standard deviation for the intra-annual variation in the daily average normalized $P_1(1)$ OH column abundance over TMF after subtracting the linear fit to the interannual trend is about 0.12 and the peak-to-peak amplitude of the daily average variation is ~30–35%.

[19] The morning and afternoon daily average normalized $Q_1(2)$ OH column abundances also are highly correlated (Figure A12), but the correlation is not as good as for the $P_1(1)$ OH line and the slope for the fit relating the morning and afternoon daily averages (equation (6)) differs from 1.0 by a statistically significant amount.

$$a_{0n} = 0.80(\pm 0.07)m_{0n} + 0.00(\pm 0.01) \quad (6)$$

where a_{0n} = daily average normalized afternoon $Q_1(2)$ OH column abundance and m_{0n} = daily average normalized morning $Q_1(2)$ OH column abundance. There is a correlation between the daily average normalized OH columns from the $P_1(1)$ and $Q_1(2)$ OH lines (Figure A13), but the slope for the fit relating the $P_1(1)$ and $Q_1(2)$ results (equation (7)) differs from 1.0 by a statistically significant amount.

$$d_{0n} = 0.82(\pm 0.04)d_{1n} + 0.00(\pm 0.01) \quad (7)$$

where $d_{1n} = P_1(1)$ daily average normalized OH column and $d_{0n} = Q_1(2)$ daily average normalized OH column. This indicates the deviations from the mean for the $Q_1(2)$ OH line are typically only 82% of those for the $P_1(1)$ OH line.

[20] The differences between the results from the $P_1(1)$ and $Q_1(2)$ lines can be partially attributed to differences in removing the background solar Fraunhofer spectrum, but other possible sources for the observed differences are still

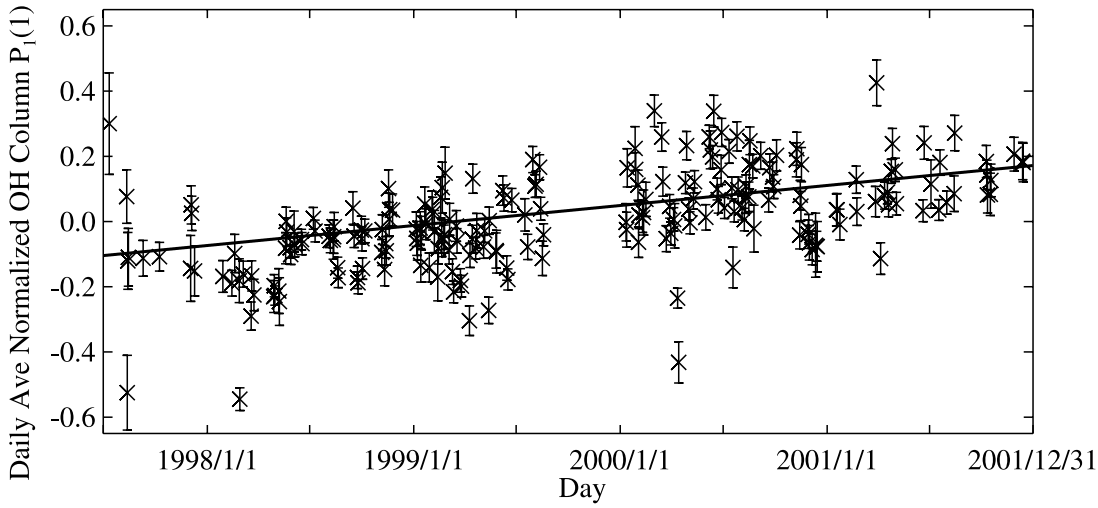

Figure 3. Daily average of normalized OH column measurements over TMF for the $P_1(1)$ OH line at 10°–65° SZA. Uncertainties are $2\sigma_r$ uncertainties on the mean for each day. The line indicates a linear least squares fit to the data.

under review. On the basis of the known difficulties in properly removing the background solar Fraunhofer spectrum from the $Q_1(2)$ line measurements and the statistical analyses described above, the $Q_1(2)$ line measurements have not been used in the modeling portion of the present study. The recently revised line strengths [*Gillis et al.*, 2001] should not significantly alter the normalized OH column abundances.

4. Photochemical Models

[21] Two photochemical models were used to interpret the intra-annual variations observed in the OH column over TMF: The Caltech/JPL numerical model [*Allen et al.*, 1981] and an analytic model [*Pickett and Peterson*, 1996]. The numerical model provided estimates of the expected photochemical state of the atmosphere at selected solar zenith angles and the analytic model was used for sensitivity (perturbation) calculations about the numerical model results. The analytic model was more convenient for the sensitivity calculations than the numerical model because the analytic model does not incorporate the automated feedback processes that are present in the numerical model. Thus each of the parameters affecting OH concentrations could be varied independently.

[22] The numerical model was initialized using species profiles measured by the Atmosphere Trace Molecule Spectroscopy (ATMOS) Experiment in 1985 [*Allen and Delitsky*, 1991]. The one-dimensional numerical model was run to diurnally averaged steady state with vertical eddy diffusion, then run in a diurnally varying mode with no transport until the OH concentrations at all model levels between 0 and 84 km altitude were diurnally repetitive to within 0.5%. The kinetic rates and photolysis cross sections [*DeMore et al.*, 1997], transmission and absorption in the O_2 Schumann-Runge Band [*Allen and Frederick*, 1982; *Froidevaux et al.*, 1985], and the solar fluxes [*Allen and Delitsky*, 1991] were standard values and parameterizations for the Caltech/JPL model. The curvature of the Earth's atmosphere and local sunrise/sunset were accounted for in determining the photolysis rates at each altitude. Recently recommended changes in kinetic rates [*Sander et al.*, 2000] do not have a significant impact on the present calculations (section 5).

[23] The analytic photochemical model used for the present study was based on that developed by *Pickett and Peterson* [1996]. The primary assumptions are the same as for their model: (1) OH, H, and HO_2 are in photochemical steady state, (2) HNO_3 is in photochemical steady state, (3) $O(^3P)$ and $O(^1D)$ are in photochemical steady state, and (4) each CH_3 radical produced is assumed to give a net yield of one HO_2 from subsequent (unmodeled) reactions. The analytic model includes no vertical transport. The nominal concentrations (except that for OH), kinetic reaction rates, and photolysis rates at all altitudes were taken from the numerical model. The analytic model assumes production of HO_x (= H + OH + HO_2) is dominated by photolysis of H_2O and reactions of $O(^1D)$ with H_2O and CH_4. Loss of HO_x is assumed to be dominated by reaction of OH with HO_2. Reactions of OH with NO_2 to form HNO_3 and of OH with HNO_3 were also included. The photolysis and kinetic reactions included in the analytic model are given in Table 1. The reaction numbering system used by *Pickett and Peterson* [1996] has been adopted for the present analytic model. The analytic model's absolute OH concentrations agreed well ($\leq$5% difference) with those from the numerical model at 30–60 km altitude at all three solar zenith angles that were used for the sensitivity analyses (morning 60°, noon, and afternoon 65°). At noon, the analytic model's absolute OH concentrations were within 5% of the numerical model's at 25–70 km altitude. Differential calculations, such as those used in section 6, should agree even more closely for the two photochemical models at 25–70 km altitude where 65–70% of the OH column lies.

Table 1. Reactions for the Analytic OH Model

Reaction										Rate Constant[a]
O_3	+	hν			→	$O(^1D)$	+	$O_2(^1\Delta)$		J_{1a}
O_3	+	hν			→	$O(^1D)$	+	O_2		J_{1b}
O_3	+	hν			→	O	+	O_2		J_2
H_2O	+	hν			→	OH	+	H		J_3
HNO_3	+	hν			→	OH	+	NO_2		J_4
$O(^1D)$	+	N_2			→	O	+	N_2		k_{1a}
$O(^1D)$	+	O_2			→	O	+	O_2		k_{1b}
$O(^1D)$	+	H_2O			→	2	OH			k_2
OH	+	HO_2			→	H_2O	+	O_2		k_3
O	+	O_2	+	N_2	→	O_3	+	N_2		k_{4a}
O	+	O_2	+	O_2	→	O_3	+	O_2		k_{4b}
OH	+	O			→	H	+	O_2		k_5
OH	+	O_3			→	O_2	+	HO_2		k_6
OH	+	CO			→	H	+	CO_2		k_7
HO_2	+	O			→	OH	+	O_2		k_8
HO_2	+	O_3			→	OH	+	2 O_2		k_9
HO_2	+	NO			→	OH	+	NO_2		k_{10}
OH	+	HNO_3			→	H_2O	+	NO_3		k_{11}
H	+	O_3			→	OH	+	O_2		k_{12}
H	+	O_2	+	M	→	HO_2	+	M		k_{13}
OH	+	NO_2	+	M	→	HNO_3	+	M		k_{14}
$O(^1D)$	+	CH_4			→[b]	OH	+	CH_3		k_{15}
OH	+	CH_4			→[b]	H_2O	+	CH_3		k_{16}

[a]Reaction numbering system is same as that used by *Pickett and Peterson* [1996].

[b]A net yield of one HO_2 per CH_3 radical produced was assumed, as was done by *Pickett and Peterson* [1996].

[24] The present analytic model differs in three ways from the *Pickett and Peterson* [1996] model. First, the spin-forbidden channel for O_3 photolysis was included, photolysis reaction 1b. Second, the different efficiencies for N_2 and O_2 as third bodies were included for kinetic reactions 1 and 4. Third, kinetic reaction 1 was included properly as a source of $O(^3P)$ atoms. Equation (2) of *Pickett and Peterson* [1996] is therefore modified to be

$$[O] = \frac{(J_{1a} + J_{1b} + J_2)[O_3]}{(k_{4a}[N_2] + k_{4b}[O_2])[O_2]} \quad (8)$$

None of the subsequent equations in *Pickett and Peterson* [1996] are affected by this correction, but the O and OH concentrations from the present model will differ by a small amount from those calculated using the *Pickett and Peterson* [1996] model.

[25] For the assumptions stated above, the OH concentration is determined by finding the positive root of equation (9) [*Pickett and Peterson*, 1996]. Solutions for this equation were computed numerically.

$$\alpha[OH]^2 + \beta[OH] + \gamma = 0 \quad (9)$$

where

$$\alpha = \frac{k_3 c_2}{c_1} \tag{10}$$

$$\beta = k_{11}[\mathrm{HNO_3}] - \frac{k_3 c_3}{c_1}[\mathrm{H_2O}] \tag{11}$$

$$\gamma = -\left(J_3 + \frac{(J_{1a}+J_{1b})k_2[\mathrm{O_3}]}{(k_{1a}[\mathrm{N_2}]+k_{1b}[\mathrm{O_2}])}\right)[\mathrm{H_2O}] - \frac{(J_{1a}+J_{1b})k_{15}[\mathrm{O_3}][\mathrm{CH_4}]}{(k_{1a}[\mathrm{N_2}]+k_{1b}[\mathrm{O_2}])} \tag{12}$$

$$c_1 = \frac{k_8(J_{1a}+J_{1b}+J_2)[\mathrm{O_3}]}{(k_{4a}[\mathrm{N_2}]+k_{4b}[\mathrm{O_2}])[\mathrm{O_2}]} - k_9[\mathrm{O_3}] + k_{10}[\mathrm{NO}] \tag{13}$$

$$c_2 = k_6[\mathrm{O_3}] + \frac{fk_5(J_{1a}+J_{1b}+J_2)[\mathrm{O_3}]}{(k_{4a}[\mathrm{N_2}]+k_{4b}[\mathrm{O_2}])[\mathrm{O_2}]} + fk_7[\mathrm{CO}] + k_{16}[\mathrm{CH_4}] + k_{11}[\mathrm{HNO_3}] \tag{14}$$

$$c_3 = (1-f)J_3 + \frac{k_2(J_{1a}+J_{1b})[\mathrm{O_3}]}{(k_{1a}[\mathrm{N_2}]+k_{1b}[\mathrm{O_2}])} \tag{15}$$

$$f = \frac{k_{13}[\mathrm{O_2}][M]}{k_{12}[\mathrm{O_3}]+k_{13}[\mathrm{O_2}][M]} \tag{16}$$

[26] Simplified approximations to the full solution for equation (9), such as equations (17), (18), and (19), help in understanding the physical quantities that control OH concentrations in different regions of the atmosphere. Equations (17), (18), and (19) were derived from the full analytic model by retaining only the largest term(s) in the solution at the specified altitudes. The two largest terms were retained if the difference between them was less than a factor of 3.

$$[\mathrm{OH}](30-35\ \mathrm{km}) \approx \sqrt{\left(\frac{k_2 J_{1a}[\mathrm{H_2O}]}{k_3 k_6 k_{1a}[\mathrm{N_2}]}\right)\left(k_{10}[\mathrm{NO}] + \frac{k_8(J_{1a}+J_2)[\mathrm{O_3}]}{k_{4a}[\mathrm{N_2}][\mathrm{O_2}]}\right)} \tag{17}$$

$$[\mathrm{OH}](40-60\ \mathrm{km}) \approx \sqrt{\left(\frac{k_8[\mathrm{H_2O}]}{k_3 k_5}\right)\left(\frac{k_2 J_{1a}[\mathrm{O_3}]}{k_{1a}[\mathrm{N_2}]} + J_3\right)} \tag{18}$$

$$[\mathrm{OH}](65-80\ \mathrm{km}) \approx \sqrt{\left(\frac{k_8 J_3[\mathrm{H_2O}]}{k_3 k_5}\right)} \tag{19}$$

On the basis of these approximate solutions to the analytic model, we expect $[\mathrm{OH}] \propto \sqrt{([\mathrm{H_2O}])}$ at 30–80 km altitude. This agrees with previous calculations for the stratosphere and mesosphere [*Canty and Minschwaner*, 2002]. Similarly, the analytic model predicts that $[\mathrm{OH}] \propto \sqrt{([\mathrm{O_3}])}$ at 40–55 km altitude, but not at other altitudes. Above 55 km, production of HO_x is increasingly dominated by J_3; below 40 km, [OH] is dependent on both $[O_3]$ and [NO].

5. Model Sensitivity Analyses

[27] Sensitivity calculations using the analytic model were examined to identify the physical quantities that are expected to control the OH column abundance and to assess quantitatively how well the observed variations in the OH column over TMF could be explained by observed variations in controlling species, such as H_2O and O_3. The analytic model was more convenient for this purpose than the numerical model because the analytic model does not incorporate the automated feedback processes that are present in the numerical model. Thus each of the parameters affecting OH concentrations could be varied independently.

[28] Linear sensitivity coefficients for each of the controlling species in equation (9) were calculated at each altitude using equation (20).

$$S_{ij} = \frac{\Delta\left(\ln[\mathrm{OH}]_j\right)}{\Delta\left(\ln[i]_j\right)} \tag{20}$$

where j defines the altitude layer within the analytic model, i is the controlling species whose abundance is being varied, and ln is the natural logarithm. Equation (20) assumes the response function is linear and the tests we conducted by perturbing the concentrations of H_2O, O_3, NO, CH_4, HNO_3, and CO by ±10% and ±25% indicate there are no significant deviations from linearity over this range.

[29] In addition to the "local" effect of changes in the controlling species on the OH concentration, the partial column of O_3 above each altitude affects the radiation field at lower altitudes and thus affects the production rate for OH via the production of $O(^1D)$. The photolysis rate for production of $O(^1D)$ from O_3 is governed by the optical depth above each level in the atmosphere which is controlled primarily by the overhead partial column of O_3 for the relevant wavelengths. For example, if the O_3 above 40 km altitude is decreased uniformly by 25%, then the optical depth above 40 km altitude will be decreased by 25%. This will increase the actinic flux at 40 km altitude that can photolyze O_3 to produce $O(^1D)$ and thus will increase the photolysis rate, J_1, at 40 km altitude. A larger value for J_1 at 40 km altitude will increase the OH concentration at 40 km altitude. Thus a decrease in the O_3 overhead above 40 km altitude leads to an increase in the OH concentration at 40 km altitude and an increase in the OH column abundance. Consequently, the "local photolytic" and "radiative" effects of changes in O_3 concentrations have opposite sign and, as will be shown, can mostly cancel each other when integrated over the entire column. Because the overhead partial column of O_3 determines the radiation field at each level at the relevant wavelengths for production of $O(^1D)$ and because O_3 concentrations can be observed remotely (e.g., by HALOE) while vertical profiles of the actinic flux are not typically measured, the sensitivity of the OH column to the actinic flux has been expressed in terms of the overhead partial column of O_3 ("OverO_3") (equation (21)).

$$S_j(\mathrm{Over O_3}) = \frac{\Delta\left(\ln[\mathrm{OH}]_j\right)}{\Delta\left(\ln(J_{1a}+J_{1b})_j\right)} \frac{\Delta\left(\ln(J_{1a}+J_{1b})_j\right)}{\Delta\left(\ln(\mathrm{Over O_3})_j\right)} \tag{21}$$

The relationship between J_1 and OH was approximately linear over the ±25% range that was examined but the relationship between J_1 and "OverO_3" was not. This is the only significant uncertainty in any of the derived sensitivity coefficients other than the limitations imposed by the assumptions used in deriving the analytic model.

[30] To determine the effect that a change in a physical quantity at any altitude will have on the OH column, the sensitivity coefficient, S_{ij}, must be multiplied by the fraction of the OH column at that altitude to derive a weighting function (equation (22)).

$$W_{ij} = S_{ij} \frac{[\mathrm{OH}]_j \Delta z_j}{\Sigma [\mathrm{OH}]_j \Delta z_j} \tag{22}$$

where Δz_j is the thickness of the altitude layer. The thickness of all altitude layers was 2 km for all of our calculations.

[31] The weighting function, W_{ij}, can be multiplied by the observed fractional change in a controlling species, i, at any altitude to determine the expected fractional change in the OH column. The expected fractional change in the OH column due to changes in multiple controlling species is then given by equation (23).

$$\Delta(\ln \mathrm{OH}_c) = \Sigma_j \Sigma_i \Delta\left(\ln[i]_j\right) W_{ij} \tag{23}$$

where OH_c is the OH column abundance. The weighting functions thus can be combined with observed changes in species concentrations (e.g., from HALOE) to calculate the expected fractional change in the OH column for comparison with the observed daily average variations as is discussed in the next section.

[32] As an initial assessment of which controlling species have significant influence on the OH column abundance, column sensitivity coefficients were calculated using equation (24).

$$S_{ic} = \Sigma_j \frac{\Delta\left(\ln[\mathrm{OH}]_j\right)}{\Delta\left(\ln[i]_j\right)} \frac{[\mathrm{OH}]_j \Delta z_j}{\Sigma [\mathrm{OH}]_j \Delta z_j} \tag{24}$$

where the fractional change in $[i]_j$ was assumed to be the same at all altitudes, ±25%. This range encompasses the range of variability expected for the primary physical quantities. The results from these column sensitivity calculations (Table 2, column 2) are normalized so they indicate the fractional change in the OH column abundance that would result if each physical quantity was changed by 100% at all altitudes (0–130 km). A negative sensitivity coefficient means the OH column change is opposite in sign to the change in that physical quantity. Column sensitivity coefficients for three times of day (morning at 60° SZA, noon at 30° SZA, and afternoon at 65° SZA) were calculated using OH profiles that span the range of measurements reported by *Pickett and Peterson* [1996] and *Conway et al.* [2000]. Column sensitivity coefficients also were calculated for the noontime cases using recently proposed alternate kinetic rates [*Sander et al.*, 2000, 2002; *Summers et al.*, 1997]. The differences for H_2O, O_3, "OverO_3," and NO from the results in Table 2, column 2, were no more than 2%. The three parameters that are predicted to have the greatest influence on the OH column abundance are $[H_2O]$, $[O_3]$, and "OverO_3," as expected [*Pickett and Peterson*, 1996].

[33] The sensitivity coefficients (Figure 4) are independent of the OH profile but may vary during a day if the dominant chemistry at an altitude changes. Most were found to vary only slightly throughout the range of SZA at which the OH column measurements over TMF are made, such as those in Figures A14 and A15. The sensitivity coefficient for "OverO_3" does vary significantly with the time of day (Figure A16). The sensitivity coefficients with the largest magnitudes are found at 15–20 km altitude where OH concentrations are most sensitive to the concentrations of

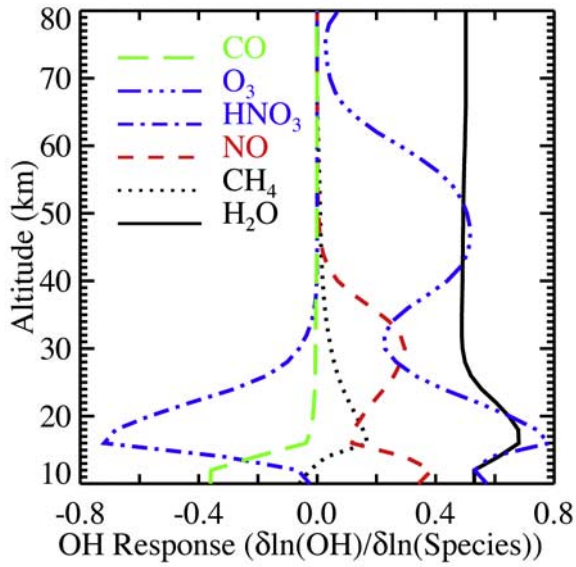

Figure 4. Sensitivity coefficients calculated as described in the text from the analytic model for changes in the concentrations of the species that are expected to influence OH concentrations at each altitude. All sensitivity coefficients were calculated for noontime conditions at spring equinox near 30°N latitude. The long-dashed line is for CO, the dash-dot-dot-dot line is for O_3, the dash-dot line is for HNO_3, the short-dashed line is for NO, the dotted line is for CH_4, and the solid line is for H_2O.

Table 2. Sensitivity of Modeled OH Column

Physical Quantity[a]	Range of Column Sensitivity Coefficient[b]	Expected Variation[c]	Range of Calculated OH Column Response[d]
H_2O	49–51%	±25%	±12%
O_3	35–45%	±25%	±(9–11)%
NO	4–11%		
CO	−1 to −3%		
HNO_3	−1 to −5%		
CH_4	0.8–1.2%		
OverO_3	−26 to −89%	±25%	±(−7 to −22)%

[a]Physical quantity that was varied in the sensitivity calculation. Species abundances were changed at 0–130 km altitude. "OverO_3" is the partial column abundance of O_3 above each layer in the photochemical model. "OverO_3" was varied to determine the effect of changes in the radiation field on [OH].

[b]Linearized OH column sensitivity coefficients (S_{ic}) computed using equation (24) and multiplied by 100 to express as a percentage. Values are a range, where the range encompasses the results from all six weighting functions shown in Figure 5.

[c]Expected typical range of variability for the parameter within the 11–81 km altitude region ($\Delta(ln[i])_c$) expressed as a percentage.

[d]Calculated change induced in OH column abundance ($= S_{ic} \times \Delta(ln[i])_c$) based on the expected variation in column 3.

HNO_3, H_2O, and O_3. At higher altitudes, where a majority of the OH column is predicted to be, OH concentrations are most sensitive to the concentrations of H_2O and O_3 with a weaker sensitivity to NO.

[34] The weighting functions are dependent on the shape of the OH profile. Three OH profiles that span the range of OH profiles (Figure A17) were selected for calculating the weighting functions for H_2O, O_3, and "OverO_3" (Figure 5). The dependence on the shape of the OH profile is particularly significant for the H_2O weighting function above 45 km altitude, and for H_2O and O_3, the weighting functions are significantly more sensitive to the OH profile than the smaller variations of the sensitivity coefficients with time of day. The weighting function for "OverO_3" has comparable sensitivity to both the OH profile and the time of day (Figure 5a), and the weighting function for "OverO_3" is negative at most altitudes. The magnitude of the weighting function for "OverO_3" is approximately equal to that for O_3 in the stratosphere, but the weighting function for "OverO_3" has a greater dependence on the shape of the OH profile than is true for the O_3 weighting function. Consequently, the net effect of changes in O_3 concentrations will depend on the shape of the OH profile.

6. Discussion

6.1. Comparison With Other Available OH Column Measurements

[35] Column OH abundances have been measured over a number of sites as noted in section 1. The four sites at which measurements have been made regularly for more than a year are Fritz Peak Observatory (FPO), Colorado, New Mexico Institute of Mining and Technology (NMT), New Mexico, University of Tokyo (Tokyo), Japan, and Table Mountain Facility (TMF), California. Significant, possibly systematic, differences have been noted among the column OH abundances measured over these sites [*Mills et al.*, 2002; *Iwagami et al.*, 1998]. To minimize the sensitivity to systematic errors, the present analysis has focused on the variations observed in the normalized OH column (i.e., deviations from the mean). A comparable analysis has not been completed for the Tokyo

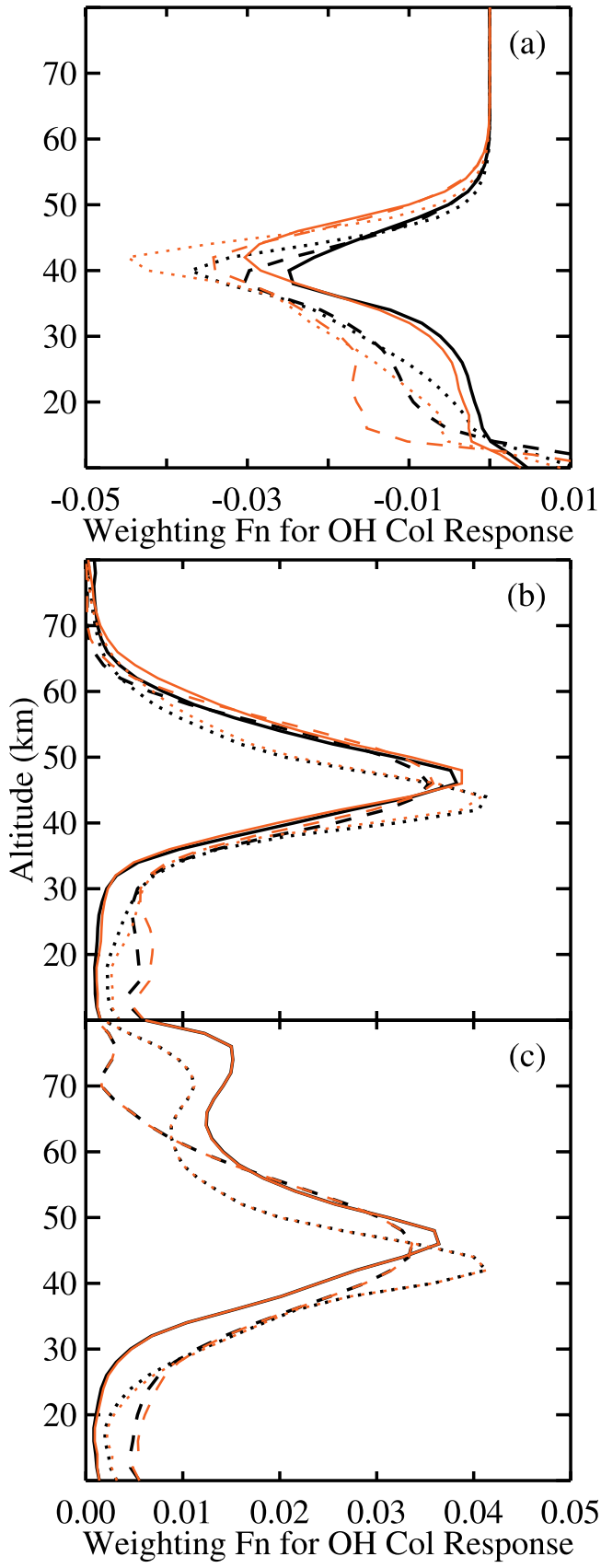

Figure 5. (opposite) Weighting functions as defined in the text that give the response of the OH column to changes in (a) "OverO_3" and to changes in (b) O_3 and (c) H_2O concentrations as a function of altitude for three OH profiles and two times of day. The noontime sensitivity coefficients were used for the curves shown in black, and the afternoon sensitivity coefficients were used for the curves shown in red (Figures A14, A15, and A16). The short-dashed line uses the empirical high-Sun OH profile from *Canty et al.* [2000], the dotted line uses the lower limit OH profile from MAHRSI's 1997 measurements [*Conway et al.*, 2000], and the solid line uses the OH profile from the February 1992 model calculation of *Pickett and Peterson* [1996]. These OH profiles span the expected range (Figure A17). For "OverO_3" the differences between noon and afternoon are comparable in magnitude to the differences among the OH profiles. For O_3 and H_2O, the noon and afternoon curves are almost indistinguishable for almost all altitudes and all OH profiles.

data, and the published Tokyo data do not permit a detailed analysis similar to what has been presented here. However, the peak-to-peak intra-annual variation in $P_1(1)$ OH column abundance observed "near-noon" over Tokyo in 1992–1995 [*Iwagami et al.*, 1998] is similar to that observed over TMF in 1997–2001. The FPO and NMT data have been analyzed using a methodology that is similar to that used in the present study, and T. Canty (personal communication, 2003) provided the monthly average normalized $P_1(1)$ OH column abundances measured over FPO for the August 1997 to November 2000 time period [*Canty and Minschwaner*, 2002] for comparison with the TMF measurements over that time period. The variability about a linear fit to the monthly average FPO data obtained from August 1997 to November 2000 has a standard deviation of 0.07. The variability about a linear fit to 30-day averages of the normalized $P_1(1)$ TMF OH data from August 1997 to November 2000 has a standard deviation of 0.08. A linear fit to the FPO data from August 1997 to November 2000 suggests an increase in the OH column abundance over FPO of about 30% (difference divided by mean) over this time period. The corresponding increase over TMF for the same time period based on the linear fit in Figure 3 is 20%. The difference in statistical variability is within the combined uncertainties on the two data sets. The difference in the magnitude of the interannual trends is not within the combined statistical uncertainties. This difference should be examined in greater detail after data has been collected for a longer time period over TMF to assess its geophysical significance.

6.2. Measured Interannual and Intra-annual OH Column Variations

[36] As shown in section 3, the OH column abundance over TMF increased by about 25% (difference divided by mean) from July 1997 to December 2001. A similar interannual trend has been reported for the OH column abundance observed over FPO for 1997–2000 [*Canty and Minschwaner*, 2002]. The measurement time period of the current TMF data set is too short to provide a definitive conclusion regarding the cyclicality, amplitude, correlation with solar cycle, or origin of the observed interannual trend. However, if the interannual variation is cyclical and is connected to the solar cycle, then the amplitude of the increase in OH column abundance that was observed over TMF from 1997 to 2001 is at least a factor of 2 larger than model calculations predict (~5–10% difference from solar maximum to minimum) [*Mills et al.*, 2002; *Canty and Minschwaner*, 2002].

[37] On intra-annual timescales, statistically significant deviations from the empirical mean OH column of up to +40% and −50% are observed and variability on at least week-to-week or monthly timescales is readily apparent, section 3. As is also discussed in section 3, the observed variations in OH column appear to occur "uniformly" throughout the day. Our attempts to model the observed intra-annual variations are the subject for the remainder of section 6.

6.3. OH Column Variations Inferred From Measurements of Precursors

[38] The model sensitivity analyses in section 5 suggest that the observed intra-annual variations in OH column abundance should be caused primarily by variations in the concentration of H_2O and to a lesser extent O_3. The remainder of this section compares the OH column abundance variations observed over TMF with those expected on the basis of observed variations in the concentrations of H_2O and O_3 near TMF and the weighting functions derived in section 5. These comparisons are limited by the quality of the OH, H_2O, and O_3 measurements and by the degree to which these measurements are spatially and temporally coincident. The stratospheric ozone LIDAR at TMF can only measure O_3 up to ~50 km [*Leblanc and McDermid*, 2000]. The Naval Research Laboratory's (NRL) Water Vapor Millimeter-wave Spectrometer (WVMS) at TMF can only provide H_2O concentrations above 45 km altitude [*Nedoluha et al.*, 1995] and was not operating properly for at least 1998–2001. The Microwave Limb Sounder (MLS) aboard the Upper Atmosphere Research Satellite (UARS) [*Barath et al.*, 1993] was operated very sporadically in 1997–2001 and one of its primary O_3 measurement channels was not functioning. The Stratospheric Aerosol and Gas Experiment (SAGE) II does not provide H_2O or O_3 concentrations above 50 km altitude [*Zaun et al.*, 1983]. Consequently, the only data set we found that provided measurements of H_2O and O_3 over the altitude range of at least 15–80 km for 1997–2001 was from the Halogen Occulation Experiment (HALOE) [*Russell et al.*, 1993].

[39] HALOE measures species concentrations via sunrise and sunset occultations. We first selected all occultations that met our criteria (defined later) for spatial and temporal coincidence with the TMF OH column measurements. We then interpolated the measured HALOE (v. 19) concentrations onto a 2-km altitude grid from 12 to 80 km to match the grid used for the modeling. We divided the concentration at each altitude by the mean concentration measured at that altitude during the period July 1997 to December 2001. The measured vertical profiles of concentrations were thus converted into vertical profiles of the fractional deviation from the mean for each species. This was done separately for the sunrise and sunset occultations, but no significant differences in the temporal behavior of the sunset and sunrise data were evident. These fractional deviations from the mean are analogous to the normalized OH column abundances discussed in section 3 and are referred to hereafter as "normalized" species concentrations. The normalized species concentrations were multiplied by the altitude-dependent weighting functions (Figure 5) and summed as described by equation (23) to calculate the expected value for the normalized OH column on each day. The 2-σ uncertainties on the HALOE measurements of each species at each altitude were converted into 2-σ uncertainties on the normalized deviation from the mean using standard methods for propagating uncertainties [*Bevington*, 1969]. The 2-σ uncertainty on the calculated normalized OH column abundance for each species was then determined in the standard manner [*Bevington*, 1969] by multiplying the uncertainty at each altitude by the weighting function for that altitude and summing the weighted uncertainties over all altitudes.

[40] Figure 6 shows the separate contributions from the normalized variations in H_2O, O_3, and "OverO_3" when summed over the 11–81 km altitude region. A clear annual cycle is evident in all three contributions to the calculated

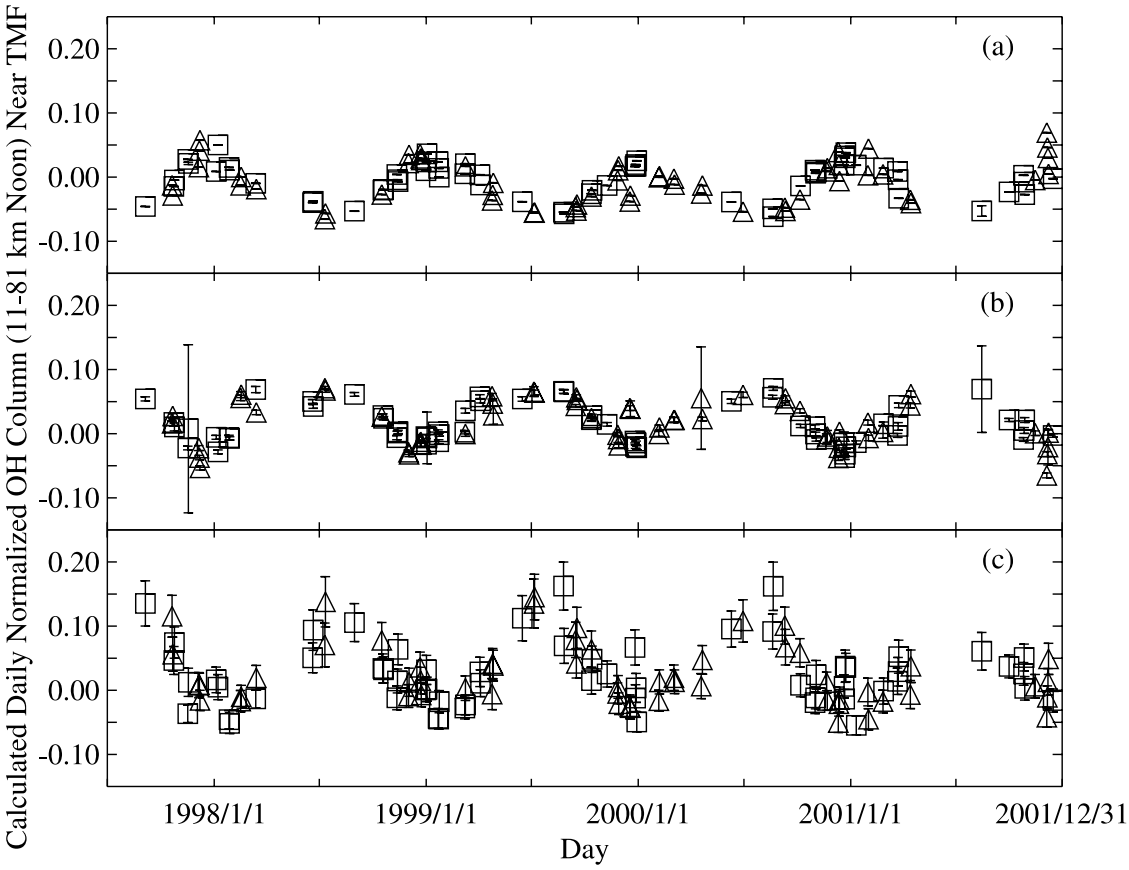

Figure 6. Daily average normalized OH columns calculated as described in the text based on the observed deviations from the mean H_2O and O_3 profiles for (a) "OverO_3," (b) O_3, and (c) H_2O. The OH column variations were inferred on the basis of the noontime sensitivity coefficients (Figures A14, A15, and A16) and the nominal OH profile from MAHRSI's 1997 measurements [*Conway et al.*, 2000]. All H_2O and O_3 observations obtained by HALOE (v. 19) on a single day within 5° latitude and 10° longitude of TMF at 11–81 km altitude were averaged to create the daily average H_2O and O_3 profiles. Uncertainties are 2σ uncertainties from the HALOE measurements. The uncertainties in the weighting functions were not included. Triangles indicate that the HALOE measurements are from sunrise occultations, and squares indicate that the HALOE measurements are from sunset occultations.

OH column, but there is no corresponding clear signature of an annual cycle in the observed daily average OH column variations (Figure 3). It is also evident from Figure 6 that the contributions to the expected OH column variation from the normalized variations in O_3 and "OverO_3" are opposite in sign and approximately equal in magnitude on a column-integrated basis. Consequently, the contributions to the calculated OH column from O_3 and "OverO_3" should approximately cancel on a column-integrated basis and the calculated OH column variations should be dominated by the contribution from the normalized variations in H_2O.

[41] Figure 7 shows the calculated OH column variations using the noon weighting functions. Each of these calculations is the sum of the contributions due to variations in H_2O, O_3, and "OverO_3" at 11–81 km. The 2-σ uncertainties shown in Figure 7 are the root-sum-square of the 2-σ uncertainties calculated for each of the three contributors (H_2O, O_3, and "OverO_3") [*Bevington*, 1969]. The temporal pattern is similar for each of the three OH profiles, but the amplitude of the calculated OH column variation is significantly larger for the profile that has the largest fraction of the OH column in the mesosphere. Variations in the OH column are expected to be particularly sensitive to variations in mesospheric H_2O because the observed fractional variations in H_2O are larger in the mesosphere than in the stratosphere, albeit with greater uncertainties in the HALOE measurements.

6.4. Statistical Comparisons of Measurements and Model Calculations

[42] Two approaches have been taken for comparing the calculated and measured normalized OH column abundances. The first is to compare the statistical characteristics of the calculated and measured abundances. Because the normalized OH column abundances represent deviations from the mean, the primary statistical property of interest is the standard deviation for the normalized OH column abundances. The measured daily average normalized $P_1(1)$ OH column abundance over TMF has a standard deviation of 0.12. The mean $2\sigma_r$ uncertainty on the measured daily average normalized OH column abundance is 0.05 so the observed variability is much larger than the measurement

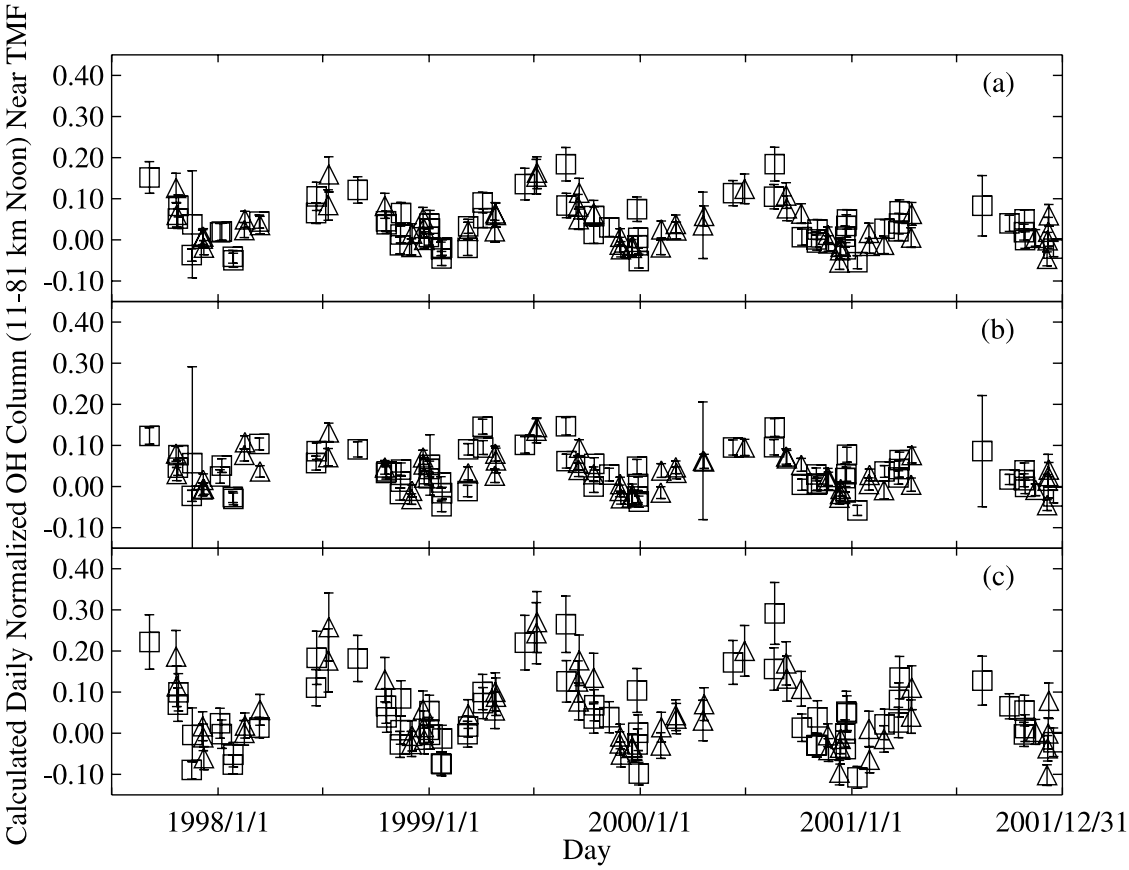

Figure 7. Daily average normalized OH columns calculated as described in the text based on the observed deviations from the mean H_2O and O_3 profiles. The OH column variations were inferred on the basis of the noontime sensitivity coefficients (Figures A14, A15, and A16) and three OH profiles that span the expected range (Figure A17). The three OH profiles illustrate the sensitivity of the calculated normalized OH column to the fraction of the OH column that is in the mesosphere: (a) the lower limit OH profile from MAHRSI's 1997 measurements [*Conway et al.*, 2000] has a moderate fraction of the OH column above 60 km altitude, (b) the empirical high-Sun OH profile from *Canty et al.* [2000] has the smallest fraction of the OH column above 60 km altitude, and (c) the February 1992 model calculation from *Pickett and Peterson* [1996] has the largest fraction of the OH column above 60 km altitude. All H_2O and O_3 observations obtained by HALOE (v. 19) on a single day within 5° latitude and 10° longitude of TMF were averaged to create the daily average H_2O and O_3 profiles. Uncertainties are 2σ uncertainties from the HALOE measurements. The uncertainties in the weighting functions were not included. Triangles indicate that the HALOE measurements are from sunrise occultations, and squares indicate that the HALOE measurements are from sunset occultations.

uncertainty. The calculated daily average normalized OH column abundance near TMF has a standard deviation of 0.05–0.09 using the noon sensitivity coefficients and 0.04–0.08 using the afternoon sensitivity coefficients. The greatest variability is found in calculations using the OH profile that has the largest fraction of the OH column in the mesosphere. The mean 2σ uncertainty on the calculated daily average normalized OH column abundance is 0.03–0.04 for both the noon and afternoon sensitivity coefficients, neglecting the uncertainties in the weighting functions. Consequently, for all three OH profiles and for both times of day, the variability in the calculated normalized OH column abundances is smaller than what is observed. The uncertainties on the measured and calculated daily average normalized OH column abundances are sufficiently small that the uncertainties cannot account for this difference between calculations and observations. Thus the greater variability in the observations is statistically significant.

[43] Three possible conclusions can be drawn from the difference between the standard deviations for the measured and calculated normalized OH column abundances. First, the fraction of the OH column in the mesosphere might be even larger than was assumed in the present study. This would contradict the results from the Middle Atmosphere High Resolution Spectrograph Investigation (MAHRSI) [*Summers et al.*, 1997] and would disagree with the conclusions reached in other studies [*Sandor and Clancy*, 1998]. Second, the sensitivity coefficients for H_2O derived from the analytic model may be a factor of 2 smaller than is true for the atmosphere. A study of interannual and seasonal variations of the OH column observed over Fritz Peak Observatory used different modeling and analysis methods,

but it also suggested that the sensitivity coefficient for H_2O should be a factor of 2 larger than predicted by present photochemical models [*Canty and Minschwaner*, 2002].

[44] Third, the observed variations in the OH column over TMF may be dominated by factors that have not been considered in the present study. One possibility is the tropospheric component of the OH column. Measurements of OH in the boundary layer have found variations in OH concentrations that could produce an ~10% change in the OH column if the variations in OH concentration that have been observed in the boundary layer are representative of the entire troposphere [*Mount et al.*, 1997; *Canty et al.*, 2000]. At present there are too few measurements of OH in the free troposphere, particularly downwind of large urban centers like Los Angeles, to corroborate or refute this hypothesis.

6.5. Comparisons of Near-Coincident Measurements and Model Calculations

[45] Our second approach for comparing the calculated and measured normalized OH column abundances has been to select coincident or near-coincident days. Initially, we attempted to compare the measured and calculated normalized OH column abundances for days on which HALOE measurements above TMF were coincident with OH column measurements over TMF. However, both data sets are sufficiently sparse that there are only 6 days from July 1997 to December 2001 with temporally and spatially coincident measurements (i.e., on the same day within 5° latitude and 10° longitude of TMF). Relaxing the temporal coincidence criterion to ±1 day produces 20 near-coincident days (Figure 8) that are grouped into 13 clusters. Relaxing the temporal coincidence to ±1 day and the spatial coincidence to ±10° latitude and any longitude produces 75 near-coincident days, but these near-coincident days are grouped into 26 clusters (with a typical interval between clusters of 1–2.5 months for the time periods where TMF data were collected regularly) and the averaged calculations may no longer be representative of the conditions at the time and location of the OH column measurements.

[46] Although some correlation between the calculated and measured normalized daily average OH column abundances is evident in Figure 8, the degree of correlation is much less than expected on the basis of the sensitivity analyses in section 5. However, the number of near-coincidences is too small to justify a definitive conclusion, particularly given the small number of near-coincidences in the months of February to October. No single weighting function (based on the three OH profiles and sensitivity coefficients from two times of day shown in Figure 5) produced a significantly better correlation between the calculated and measured normalized daily average OH column abundances than is shown in Figure 8. Time-dependent calculations using the full Caltech/JPL photochemical model for the near-coincident days would be required to assess whether the OH profile on each of the near-coincident days changes by the amount that would be required to bring a majority of the calculated OH column abundances into agreement with the measured OH column abundances. However, simulations using multiple weighting functions from Figure 5 cannot eliminate the apparent disagreement between measurements and calculations in Figure 8. These weighting functions cover a broad range of atmospheric conditions, so we believe changes in the weighting function cannot resolve the apparent disagreement between measurements and calculations.

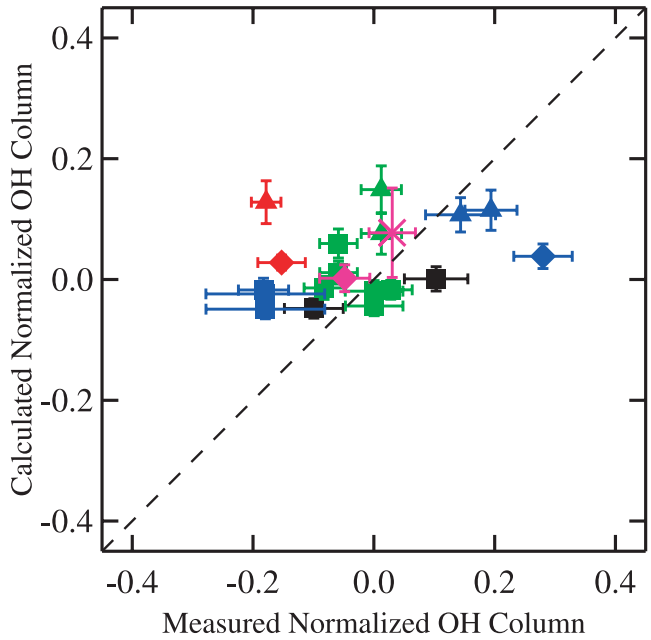

Figure 8. Calculated and measured normalized OH column abundances. The measured normalized OH column abundances are averages over 3 days. The interannual linear trend (Figure 3) has been subtracted from the measured normalized OH column abundances. The calculated normalized OH column abundances are averages over 1 day inferred from HALOE observations of H_2O and O_3 within 5° latitude and 10° longitude of TMF using the noontime sensitivity coefficients and the nominal OH profile derived from the 1997 MAHRSI measurements [*Conway et al.*, 2000]. The black squares mark data from 5 December 1997 and 27 January 1998. The green triangles mark data from 10 and 11 July 1998. The green squares mark data from 11–13 November 1998 and 21–23 January 1999. The red diamond marks the datum from 9 March 1999. The red triangle marks the datum from 15 June 1999. The blue diamond marks the datum from 2 March 2000. The blue triangles mark data from 9 and 29 June 2000. The blue squares mark data from 10–12 December 2000. The purple diamond marks the datum from 13 April 2001. The purple "X" marks the datum from 14 August 2001. The short-dashed line indicates what would be expected if the measurements and calculations agreed perfectly.

[47] The statistical comparisons in section 6.4 suggested that the actual sensitivity coefficient for variations in the concentration of H_2O ($S_j(H_2O)$) may be a factor of 2 larger than was calculated from the analytic model. This was tested by doubling $S_j(H_2O)$ at 61–81, 51–81, and 11–81 km altitude. Doubling $S_j(H_2O)$ increases the variability (one standard deviation) in the calculated normalized OH column abundance from 0.05 (using $S_j(H_2O)$ from the analytic model) to 0.08 (when doubling the sensitivity for 61–81 km), 0.08 (when doubling for 51–81 km), and 0.10 (when doubling for 11–81 km). When $S_j(H_2O)$ is doubled at

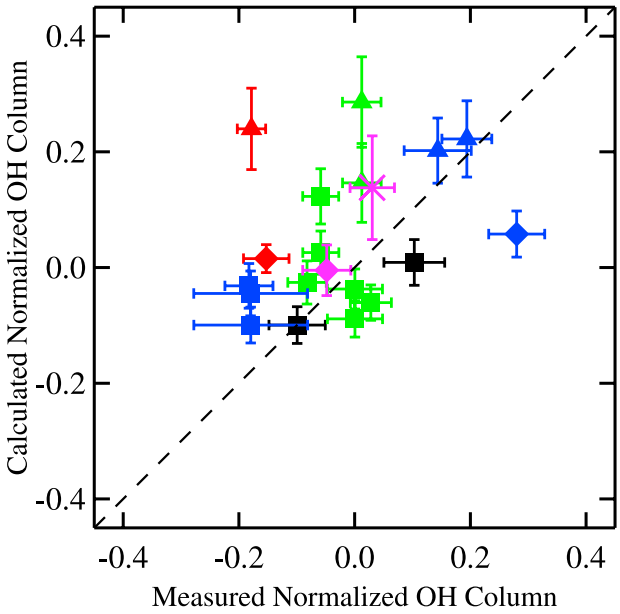

Figure 9. Same as Figure 8, but the sensitivity coefficients ($S_j(H_2O)$) for variations in H_2O concentrations at 11–81 km altitude have been doubled when determining the calculated normalized OH column abundances. The measured normalized OH column abundances are averages over 3 days. The interannual linear trend (Figure 3) has been subtracted from the measured normalized OH column abundances. The calculated normalized OH column abundances are averages over 1 day inferred from HALOE observations of H_2O and O_3 within 5° latitude and 10° longitude of TMF using the noontime sensitivity coefficients for O_3 and "OverO_3," double the noontime sensitivity coefficients for H_2O, and the nominal OH profile derived from the 1997 MAHRSI measurements [*Conway et al.*, 2000]. The black squares mark data from 5 December 1997 and 27 January 1998. The green triangles mark data from 10 and 11 July 1998. The green squares mark data from 11–13 November 1998 and 21–23 January 1999. The red diamond marks the datum from 9 March 1999. The red triangle marks the datum from 15 June 1999. The blue diamond marks the datum from 2 March 2000. The blue triangles mark data from 9 and 29 June 2000. The blue squares mark data from 10–12 December 2000. The purple diamond marks the datum from 13 April 2001. The purple "X" marks the datum from 14 August 2001. The short-dashed line indicates what would be expected if the measurements and calculations agreed perfectly. Doubling the H_2O sensitivity coefficients produces better agreement between calculations and measurements, but the scatter about the expected line is large.

11–81 km altitude, the variability in the calculated normalized OH column abundance becomes comparable to the 0.12 variability that is observed over TMF. As shown in Figure 9, however, the degree of correlation between the calculated and measured normalized OH columns does not change significantly. No single weighting function from Figure 5 produced a significantly better correlation between the calculated and measured normalized daily average OH column abundances than is shown in Figure 9. The result shown in Figure 9 plus the negative result from using multiple OH profiles for simulations (above) suggests that doubling the sensitivity coefficient for variations in H_2O will not be sufficient for resolving the differences that exist between observations and calculations. If the estimated uncertainties for the TMF measurements [*Cageao et al.*, 2001] are correct, then other factors that have not been examined in this manuscript must exert significant influence on the OH column abundance.

7. Summary and Conclusions

[48] Measurements of the OH column abundance over the Jet Propulsion Laboratory's Table Mountain Facility (TMF) have been made since July 1997 at 10°–80° solar zenith angle using a Fourier transform ultraviolet spectrometer (FTUVS). An empirical least squares fit describing the annual average OH column as a function of solar zenith angle has been derived. The measured OH column at any solar zenith angle is typically larger in the afternoon than in the morning. The variations observed in the normalized OH column abundance appear to be the result of changes in atmospheric conditions that occur on a daily or longer timescales. The magnitude of the variations observed in the daily average of the normalized OH column abundance is larger than the uncertainties on the daily averages, implying the observed variations are statistically significant.

[49] An updated analytic model that describes the OH concentration at 25–70 km altitude was derived and used to calculate sensitivity coefficients that describe how the OH concentration and the OH column abundance are expected to change in response to changes in the concentrations of H_2O, O_3, NO, CO, and CH_4. On the basis of the modeled sensitivity coefficients and HALOE observations of O_3 concentrations, the net sensitivity of the OH column abundance to variations in O_3 concentrations is close to zero because the radiative (overhead optical depth) and local photolytic effects approximately cancel when integrated over the entire column. Consequently, variations in the OH column abundance are expected to be dominated by variations in H_2O concentrations.

[50] The observed OH column over TMF increased by about 25% from July 1997 to December 2001. No significant interannual trend is apparent in the modeled OH column for this time period so the observed trend in the OH column abundance is not due to the observed interannual trends in H_2O or O_3 concentrations. The observed interannual OH column trend is at least a factor of 2 larger than the calculated difference between solar minimum and maximum. On a daily average basis, the observed variations in the normalized OH column abundance are a factor of 2 larger than calculated on the basis of HALOE observations of H_2O and O_3. This suggests that the sensitivity of OH concentrations to variations in H_2O concentrations is a factor of 2 larger than predicted in present models. However, doubling the sensitivity of OH concentrations to variations in H_2O does not, by itself, resolve the relatively poor correlation between calculated and measured normalized OH column abundances for the small number of days on which near-coincident measurements were made of OH column and H_2O and O_3 concentration profiles. These results suggest that there is some other major driver for

the observed variability in the OH column abundance that was not examined in the present study. One possibility is the troposphere. Substantial variations have been reported for OH concentrations in the boundary layer between "clean" and "urban" air, but no similar time series of measurements exists for the free troposphere.

[51] The present analysis is limited by the small number of coincident measurements of OH column abundance, H_2O, and O_3. Coincident, colocated measurements of OH column abundance along with profiles for at least 30–70 km altitude of H_2O, O_3, and temperature are needed.

[52] The OH column measurements over TMF that were described in this publication will be placed in the NDSC archive after they are brought to a consistent processing level.

8. Future Work

[53] Several types of additional measurements are required to examine questions raised in the present research. Further OH column measurements are needed to assess whether the upward trend in OH column abundance seen from 1997 to 2001 is cyclical. Two types of data intercomparisons are needed [*Mills et al.*, 2002]: (1) coincident OH column abundance and OH profile measurements and (2) intercomparisons of OH column abundances from different instruments. These intercomparisons will help resolve existing questions regarding the systematic differences between data sets. Ideally, coincident observations of OH column abundance along with vertical profiles of OH, HO_2, O_3, H_2O, and temperature over at least 30–70 km altitude are needed. This might be possible if coincident observations by Odin [*Murtagh et al.*, 2002], SABER http://asd-www.larc.nasa.gov/saber/ASDsaber.html), and SHIMMER http://uap-www.nrl.navy.mil/shimmer/shimmer.htm) can be arranged. Regular OH concentration measurements in the free troposphere, particularly downwind of large urban areas like Los Angeles, are needed to assess what fraction of the observed variability in the OH column is due to fluctuations in the OH concentration in the free troposphere.

[54] **Acknowledgments.** The research described in this paper was performed at the Jet Propulsion Laboratory, California Institute of Technology. Support received from the NASA Upper Atmosphere Research Program, the California Institute of Technology President's Fund, the Naval Research Laboratory, and NASA grants NAG1-1806 and NAG1-2151 to the California Institute of Technology is gratefully acknowledged. The authors thank Vassilli Nemtchinov and Yibo Jiang for their contributions to the collection and processing of the OH column measurements, Timothy Canty for his assistance in comparing the TMF and FPO measurements, and Fok-Yan Leung for assistance with the final versions of figures. Helpful suggestions from an anonymous reviewer are gratefully acknowledged. The HALOE data were obtained via http://haloedata.larc.nasa.gov.

References

Allen, M., and M. L. Delitsky, A test of odd-oxygen photochemistry using Spacelab-3 Atmospheric Trace Molecule Spectroscopy observations, *J. Geophys. Res.*, *96*, 12,883–12,891, 1991.

Allen, M., and J. E. Frederick, Effective photo-dissociation cross sections for molecular oxygen and nitric-oxide in the Schumann-Runge bands, *J. Atmos. Sci.*, *39*, 2066–2075, 1982.

Allen, M., Y. L. Yung, and J. W. Waters, Vertical transport and photochemistry in the terrestrial mesosphere and lower thermosphere (50–120 km), *J. Geophys. Res.*, *86*, 3617–3627, 1981.

Barath, F. T., et al., The Upper Atmosphere Research Satellite Microwave Limb Sounder instrument, *J. Geophys. Res.*, *98*, 10,751–10,762, 1993.

Bevington, P. R., *Data Reduction and Error Analysis for the Physical Sciences*, 336 pp., McGraw-Hill, New York, 1969.

Burnett, C. R., and E. B. Burnett, Spectroscopic measurements of the vertical column abundance of hydroxyl (OH) in the Earth's atmosphere, *J. Geophys. Res.*, *86*, 5185–5202, 1981.

Burnett, C. R., and E. B. Burnett, The regime of decreased OH vertical column abundances at Fritz Peak Observatory, CO: 1991–1995, *Geophys. Res. Lett.*, *23*, 1925–1927, 1996.

Burnett, C. R., and K. Minschwaner, Continuing development in the regime of decreased atmospheric column OH at Fritz Peak, Colorado, *Geophys. Res. Lett.*, *25*, 1313–1316, 1998.

Cageao, R. P., Y. L. Ha, Y. Jiang, M. F. Morgan, Y. L. Yung, and S. P. Sander, Calculated hydroxyl $A^2\Sigma^+ \rightarrow X^2\Pi(0, 0)$ band emission rate factors applicable to atmospheric spectroscopy, *J. Quant. Spectrosc. Radiat. Transfer*, *57*, 703–717, 1997.

Cageao, R. P., J.-F. Blavier, J. P. McGuire, Y. Jiang, V. Nemtchinov, F. P. Mills, and S. P. Sander, High-resolution Fourier-transform ultraviolet-visible spectrometer for the measurement of atmospheric trace species: Application to OH, *Appl. Opt.*, *40*, 2024–2030, 2001.

Canty, T., and K. Minschwaner, Seasonal and solar cycle variability of OH in the middle atmosphere, *J. Geophys. Res.*, *107*(D24), 4737, doi:10.1029/2002JD002278, 2002.

Canty, T., K. Minschwaner, K. W. Jucks, and A. K. Smith, A review of hydroxyl in the middle atmosphere: Comparison of measured and modeled vertical profiles and ground-based column observations, in *Atmospheric Science Across the Stratopause*, *Geophys. Monogr. Ser.*, vol. 123, edited by D. E. Siskind, S. D. Eckermann, and M. E. Summers, pp. 131–136, AGU, Washington, D. C., 2000.

Conway, R. R., M. E. Summers, M. H. Stevens, J. G. Cardon, P. Preusse, and D. Offermann, Satellite observations of upper stratospheric and mesospheric OH: The HO_x dilemma, *Geophys. Res. Lett.*, *27*, 2613–2616, 2000.

DeMore, W. B., S. P. Sander, D. M. Golden, R. F. Hampson, M. J. Kurylo, C. J. Howard, A. R. Ravishankara, C. E. Kolb, and M. J. Molina, *Chemical Kinetics and Photochemical Data for Use in Stratospheric Modeling: Evaluation Number 12*, *JPL Publ.*, *97-4*, 266 pp., 1997.

Froidevaux, L., M. Allen, and Y. L. Yung, A critical analysis of ClO and O_3 in the mid-latitude stratosphere, *J. Geophys. Res.*, *90*, 12,999–13,029, 1985.

Gillis, J. R., A. Goldman, G. Stark, and C. P. Rinsland, Line parameters for the $A^2\Sigma^+ - X^2\Pi$ bands of OH, *J. Quant. Spectrosc. Radiat. Transfer*, *68*, 225–230, 2001.

Hofmann, D. J., et al., Predicting future ozone changes and detection of recovery, in *Scientific Assessment of Ozone Depletion: 1998*, edited by D. L. Albritton et al., pp. 12.1–12.57, World Meteorol. Organ., Geneva, 1999.

Iwagami, N., S. Inomata, I. Murata, and T. Ogawa, Doppler detection of hydroxyl column abunance in the middle atmosphere, *J. Atmos. Chem.*, *20*, 1–15, 1995.

Iwagami, N., S. Inomata, and T. Ogawa, Doppler detection of hydroxyl column abundance in the middle atmosphere: 2. Measurement for three years and comparison with a 1D model, *J. Atmos. Chem.*, *29*, 195–216, 1998.

Jucks, K. W., D. G. Johnson, K. V. Chance, W. A. Traub, J. J. Margitan, G. B. Osterman, R. J. Salawitch, and Y. Sasano, Observations of OH, HO_2, H_2O, and O_3 in the upper stratosphere: Implications for HO_x photochemistry, *Geophys. Res. Lett.*, *25*, 3935–3938, 1998.

Leblanc, T., and I. S. McDermid, Stratospheric ozone climatology from lidar measurements at Table Mountain (34.4°N, 117.7°W) and Mauna Loa (9.5°N, 155.6°W), *J. Geophys. Res.*, *105*, 14,613–14,623, 2000.

Mills, F. P., R. P. Cageao, V. Nemtchinov, Y. Jiang, and S. P. Sander, OH column abundance over Table Mountain Facility, California: Annual average 1997–2000, *Geophys. Res. Lett.*, *29*(15), 1742, doi:10.1029/2001GL014151, 2002.

Mount, G. H., J. W. Brault, P. V. Johnston, E. Marovich, R. O. Jakoubek, C. J. Volpe, J. Harder, and J. Olson, Measurement of tropospheric OH by long-path laser absorption at Fritz Peak Observatory, Colorado, during the OH Photochemistry Experiment, Fall 1993, *J. Geophys. Res.*, *102*, 6393–6413, 1997.

Müller, R., et al., Upper stratospheric processes, in *Scientific Assessment of Ozone Depletion: 1998*, edited by D. L. Albritton et al., pp. 6.1–6.44, World Meteorol. Organ., Geneva, 1999.

Murtagh, D., et al., An overview of the Odin atmospheric mission, *Can. J. Phys.*, *80*, 309–319, 2002.

Nedoluha, G. E., R. M. Bevilacqua, R. M. Gomez, D. L. Thacker, W. B. Waltman, and T. A. Pauls, Ground-based measurements of water vapor in the middle atmosphere, *J. Geophys. Res.*, *100*, 2927–2939, 1995.

Notholt, J., H. Schutt, and A. Keens, Solar absorption measurements of stratospheric OH in the UV with a Fourier-transform spectrometer, *Appl. Opt.*, *36*, 6076–6082, 1997.

Pickett, H. M., and D. B. Peterson, Comparison of measured stratospheric OH with prediction, *J. Geophys. Res.*, *101*, 16,789–16,796, 1996.

Press, W. H., B. P. Flannery, S. A. Teukolsky, and W. T. Vetterling, *Numerical Recipes: The Art of Scientific Computing* (*FORTRAN version*), 702 pp., Cambridge Univ. Press, New York, 1989.

Russell, J. M., L. L. Gordley, J. H. Park, S. R. Drayson, W. D. Hesketh, R. J. Cicerone, A. F. Tuck, J. E. Frederick, J. E. Harries, and P. J. Crutzen, The Halogen Occultation Experiment, *J. Geophys. Res.*, *98*, 10,777–10,797, 1993.

Sander, S. P., et al., *Chemical Kinetics and Photochemical Data for Use in Stratospheric Modeling: Evaluation Number 13*, *JPL Publ.*, *00-3*, 74 pp., 2000.

Sander, S. P., et al., *Chemical Kinetics and Photochemical Data for Use in Atmospheric Studies: Evaluation Number 14*, *JPL Publ.*, *02-25*, 2002.

Sandor, B. J., and R. T. Clancy, Mesospheric HO_x chemistry from diurnal microwave observations of HO_2, O_3, and H_2O, *J. Geophys. Res.*, *103*, 13,337–13,351, 1998.

Stark, G., J. W. Brault, and M. C. Abrams, Fourier-transform spectra of the $A^2\Sigma^+ - X^2\Pi\Delta v = 0$ bands of OH and OD, *J. Opt. Soc. Am. B Opt. Phys.*, *11*, 3–32, 1994.

Summers, M. E., R. R. Conway, D. E. Siskind, M. H. Stevens, D. Offermann, M. Riese, P. Preusse, D. F. Strobel, and J. M. Russell III, Implications of satellite OH observations for middle atmospheric H_2O and ozone, *Science*, *277*, 1967–1970, 1997.

Zaun, N. H., L. E. Mauldin, and M. P. McCormick, Design and performance of the Stratospheric Aerosol and Gas Experiment-II (SAGE-II) instrument, *Proc. SPIE Int. Soc. Opt. Eng.*, *430*, 99–105, 1983.

M. Allen, Jet Propulsion Laboratory, California Institute of Technology, MS 183-401, 4800 Oak Grove Drive, Pasadena, CA 91109, USA.

R. P. Cageao and S. P. Sander, Jet Propulsion Laboratory, California Institute of Technology, MS 183-901, 4800 Oak Grove Drive, Pasadena, CA 91109, USA.

F. P. Mills, Research School of Physical Sciences and Engineering, Australian National University, Canberra ACT 0200, Australia. (frank.mills@anu.edu.au)

E. E. Remsberg, NASA Langley Research Center, MS 401B, 21 Langley Boulevard, Hampton, VA 23681, USA.

U. Richter, California Institute of Technology, M/C 138-78, 1201 E. California Boulevard, Pasadena, CA 91125, USA.

J. M. Russell III, Center for Atmospheric Sciences, Hampton University, P. O. Box 6075, Hampton, VA 23668, USA.

Y. L. Yung, California Institute of Technology, M/C 150-21, 1201 E. California Boulevard, Pasadena, CA 91125, USA.